Exploring the Light-Emitting Agents in *Renilla* Luciferases by an Effective QM/MM Approach

Ashim Nandi,[1] Aoxuan Zhang,[1] Zhen Tao Chu,[1] Wenjun Xie,[2] Zhongxin Xu,[3] Suwei Dong,[3] and Arieh Warshel[1,*]

[1] Department of Chemistry, University of Southern California, Los Angeles, California 90089-1062, United States.

[2] Department of Medicinal Chemistry, Center for Natural Products, Drug Discovery and Development (CNPD3), Genetics Institute, University of Florida, Gainesville, FL, USA.

[3] State Key Laboratory of Natural and Biomimetic Drugs, Chemical Biology Center, and School of Pharmaceutical Sciences, Peking University, Beijing, China.

* Correspondence: warshel@usc.edu

Abstract

Bioluminescence is a remarkable natural process in which living organisms produce light via specific biochemical reactions. Among these organisms, *Renilla* luciferase (RLuc), derived from the sea pansy *Renilla* reniformis, is notable for its blue light emission, making it one of the promising candidates for bioluminescent tagging. Our study focuses on RLuc8, a modified variant of RLuc characterized by eight amino acid substitutions. Recent findings have illuminated that its luminescent emitter, coelenteramide, is capable of existing in multiple protonation states. These states may significantly be influenced by adjacent proton acceptor residues at the enzyme's active site, highlighting the complex interplay between the protein structure and its bioluminescent activity. Herein employing the Quantum Mechanical Consistent Force Field (QCFF/PI) method and the semi-macroscopic Protein Dipole-Langevin Dipole method with Linear Response Approximation (PDLD/S-LRA), we show that the phenolate state of coelenteramide in RLuc8 is the predominant light-emitting species, corroborating experimental results. Our calculations also demonstrate that proton transfer from neutral coelenteramide to Asp162 is integral to the bioluminescence mechanism. Furthermore, our calculations reproduce the observed emission maximum for the amide anion in RLuc8-D120A mutant. In the case of RLuc8-D162A, we predicted that the pyrazine anion, existing in the presence of a Na^+ counterion, has an emission maximum consistent with experimental data, suggesting its primary role as potential emitter. Additionally, our calculations on the

engineered AncFT-D160A enzyme, structurally similar to RLuc8-D162A but with a significantly blue-shifted emission peak, show that the emission maximum of its neutral form of the emitter agrees well with observed data. This agreement may explain the variations in observed emission peaks. This study not only showcases an effective way for investigating the bimolecular states of chromophores in light emission but also introduces an efficient approach that integrates the proton transfer process into the calculations of the emission spectra, proving vital for further research of proton transfer and light emission in photoproteins.

Introduction

Bioluminescence is a remarkable phenomenon in which living organisms emit light as a result of a specific biochemical reaction. In recent years, bioluminescent proteins have garnered considerable attention owing to their potential applications in a variety of fields, including biosensors, biothreat assessment, and notably, as a sought-after reporter gene to observe gene expression, promoter activity, post-translational regulation assays. as well as in the realm of protein engineering.[1–6] Organisms with bioluminescence properties produce light through the oxidation of a substrate known as luciferin, a reaction that is catalyzed by a specific class of enzymes referred to as luciferases.[2,7] Among the array of bioluminescent proteins, *Renilla* luciferase (RLuc) is particularly appropriate for its applications as bioluminescent tags.[2] Unlike other bioluminescent proteins that depend on ATP, these enzymes function without ATP reliance. Instead, they require only the substrate and molecular oxygen, setting them apart in the field of bioluminescence. This 36 kDa enzyme, derived from the sea pansy, *Renilla reniformis* catalyzes the oxidation of the substrate coelenterazine, an aromatic compound specifically characterized as 2-(p-hydroxybenzyl)-6-(p-hydroxyphenyl)-8-benzylimidazo(1,2-a)pyrazine-3-(7H)-one. During the catalytic process, the substrate undergoes oxidative decarboxylation reaction, which results in the opening of the imidazole ring. This step initiates the release of carbon dioxide and the production of coelenteramide in the first singlet excited state (S_1). The

return of coelenteramide to the ground state (S_0) triggers the release of blue light, a phenomenon known as bioluminescence.[8–11] (see Scheme 1).

Several bioluminescent proteins utilize coelenterazine as a substrate, and high-resolution crystal structures have been determined for calcium-stimulated photoproteins like aequorin and obelin.[12–16] Within these proteins, coelenterazine, while not covalently attached, resides in a snug cavity. It interacts with multiple residues that contribute to the efficiency of light emission and the modulation of its color. Typically, coelenteramide, the light emitter, is thought to be deprotonated at the 6-para hydroxyphenyl group (forming a phenolate ion), a process likely facilitated by a neighboring histidine residue (His22).[14,16,17] This results in the emission of blue light in the range of 470-490 nm. However, if the emitter remains protonated, it emits a photon of purple light (405 nm).[13,16,17] Additionally, earlier studies by McCapra *et al.*[18] and Shimomura *et al.*[19] have also explored the possibility of the amide anion formed as a result of chemiluminescence[20,21] as the potential emitter. Consequently, coelenteramide is believed to exist in various bimolecular states, distinguished by their protonation states (either neutral or anionic) and the specific site of deprotonation (either phenolate or amide ion). In the presence of alkali metals, coelenteramide can also adopt a pyrazine form, where the alkali metal acts as a counter ion to the phenolate emitter, facilitating the formation of the pyrazine structure through resonance (*vide infra*).[19]

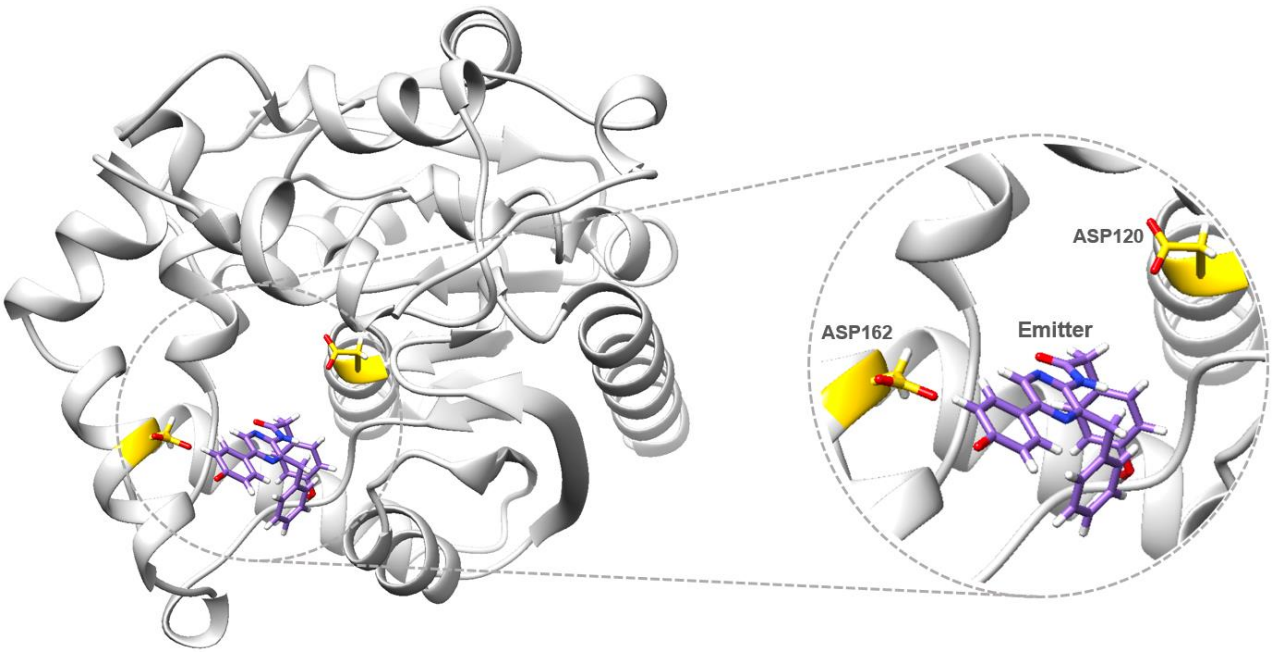

Figure 1. Schematic representation of RLuc8 (PDB entry: 7OMR), with coelenteramide as emitter, and nearby Asp162, and Asp120 residues are in sticks.

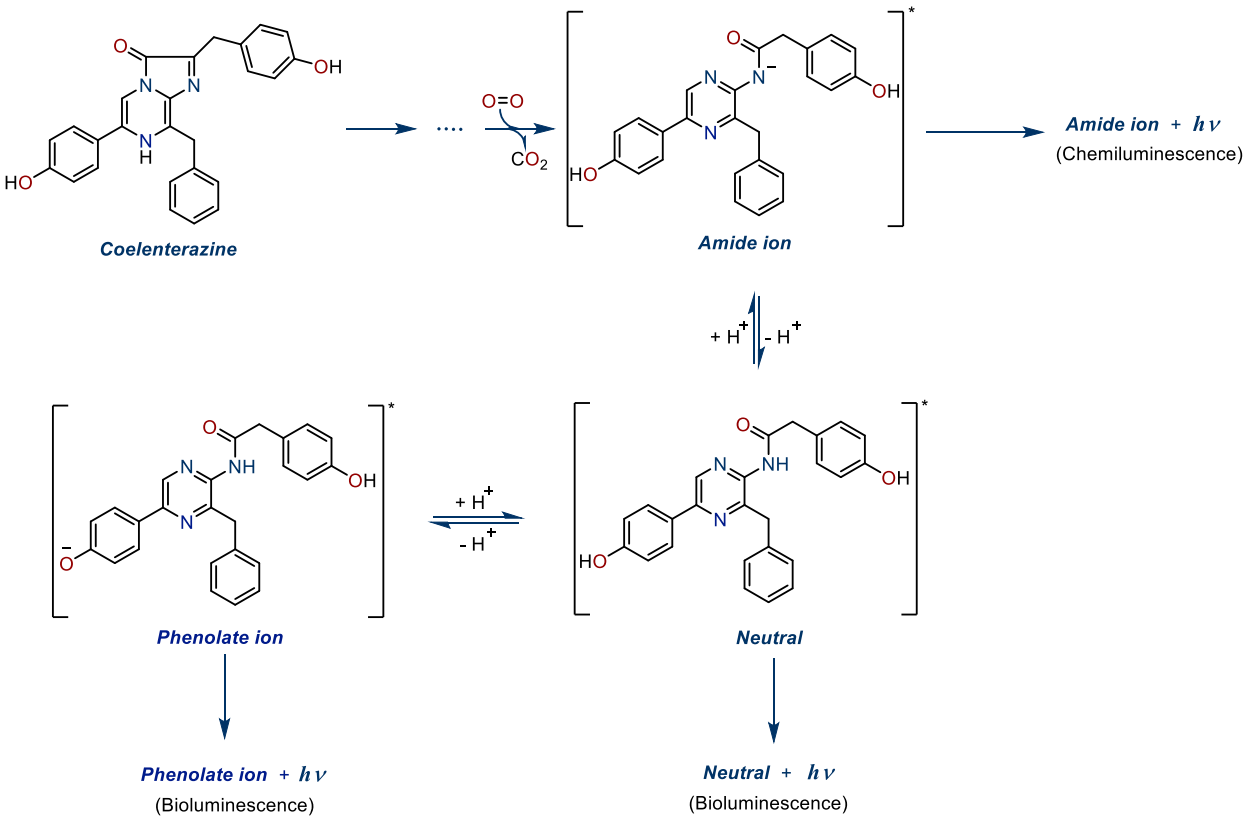

Scheme 1. Bioluminescence and Chemiluminescence path showing coelenteramide light emitter in different protonation states. The asterisk indicates molecule in the excited state. The final product is relaxed to the ground state with the emission of light ($h\nu$).

Since RLuc utilizes the same substrate as the aequorin and obelin proteins, produces identical products, and emits light with similar spectral characteristics, the reaction mechanisms are likely analogous. However, understanding the detailed catalytic mechanisms and spectral properties of RLuc has proven to be a significant challenge, largely due to the scarce availability of structural data for substrate- and product-bound enzyme complexes. To address this issue, mutagenesis experiments were conducted to create mutants that are more conducive to crystallization. In one of the earlier investigations, Loening *et al.*[22] determined the structure of a stabilized form of RLuc, which contains eight amino acid substitutions (RLuc8), both with and without the coelenteramide product bound. While the coelenteramide was found in one of these structures (PDB ID: 2PSJ), its location on the outer edge of the active site was interpreted as a nonproductive binding mode.[23] Recently, Damborsky *et al.*[24] co-crystallized coelenteramide bound RLuc8 complex with a resolution of 1.9 Å (PDB ID: 6YN2) in the presence of excess of the substrate coelenterazine, providing biological relevant structural insights. In another recent study conducted by Marek et al.,[11] a crystal structure of the RLuc8-coelenteramide complex was obtained with a high-resolution of 1.5 Å (PDB ID: 7OMR). The authors of this work carried out a detailed mechanistic study for this complex, taking into account multiple co-crystal structures of the stabilized AncFT surrogate enzyme and RLuc8 luciferases, given their structural similarities. This study was backed by mutagenesis, experimental approaches, and molecular dynamics studies. Furthermore, they assigned the bioluminescence states of the coelenteramide emitter in RLuc8 and its mutants, which is the main focus of our work.

In a study by Marek *et al*.,[11] the phenolate form of coelenteramide was identified as a potential emitter in RLuc8. This emission is hypothesized to be attributed to the deprotonation of the R2-6-(p-hydroxyphenyl) substituent, influenced by the nearby aspartic acid D162, which is only 2.9 Å away. On the other hand, the RLuc8-D162A and

RLuc8-D120A mutants see the pyrazine and amide ion as light emitters, as shown in Scheme 1. This latter finding corroborates earlier research by Shimomura and Teranishi,[20] who investigated the luminescence of various biomolecular states of coelenteramide in different solvent polarities, and in the absence of the protein environment. While the X-ray crystallography method used in the above study has provided insights into the luminescence mechanism, it is crucial to understand the molecular details associated with the luminescent reaction. This is because X-ray crystallography captures either a single spatial structure or, in the presence of defects, an average of different conformations at a specific moment in time. In particular the previous studies did not explore the relationship between the proton transfer coordinate to the emission spectra.

In this study, we explore the various biomolecular states of the coelenteramide in RLuc8 and its variants, along with their corresponding emission spectra. Furthermore, we examine the emission spectra that occur during the proton transfer process, which facilitates the transition of the chromophore from a neutral to an ionic state in RLuc8. Utilizing the quantum mechanical consistent force field (QCFF/PI) along with the semi-macroscopic protein dipole-Langevin dipole (PDLD/S) method, combined with the linear response approximation (LRA), our findings affirm the significance of the phenolate and pyrazine states of coelenteramide in RLuc8 and its D162A mutant. These states, resulting from proton transfers of neutral emitter to D162 and the presence of counter ion respectively, are pivotal for consistent bioluminescence emission energy. Notably, our computed emission wavelength for the amide ion in D120A, matches closely with experimental results. Additionally, our approach offers a robust mechanism for integrating the energetics of the proton transfer in bioluminescence reactions. This is done by determining the free energy of the reaction landscape by assessing the $\mathrm{p}K_a$ differences of the donor-acceptor proton transfer (PT) process in both the excited and ground states using the PDLD/S-LRA method (see section 2.2 and 3). This deprotonation energy is then added to the emission spectra derived from the QCFF/PI (see section 2.1). This combined approach proves to be the most effective in studying the bioluminescence process that involve proton transfer.

2. Materials and Methods

2.1. The Quantum Mechanical Consistent Force Field (QCFF/PI) Method

Understanding the bioluminescence process of the chromophore in protein environment requires a reliable QM/MM model to accurately map the excited state potential energy surface. While high-level ab initio calculations have been applied to study the spectroscopic properties of the coelenteramide emitter in the absence of protein environment, their application to studying RLuc8 with various protonation state of the emitter requires immense computational resources. A pragmatic approach is using a QM/MM variant of the semiempirical QCFF/PI method[25–27] developed in our group, which we utilized in our prior studies. For our current study, we leveraged the QCFF/PI quantum mechanical potential surface[26,28,29] combined with the protein force field of the ENZYMIX program interfaced in the MOLARIS-XG software suite.[30] Our previous studies have shown the success of this method, which integrates ENZYMIX[31] and QCFF/PI, to investigate conjugated molecules in solutions or in the presence of protein environment. An overview of our potential surface and simulation methodologies is provided below. For a deeper understanding of the QCFF/PI method, the readers are referred to the specified references [26–28,32].

The combined QM/MM potential surface for the emitter's Nth electronic excited state within its protein active site is expressed as.

$$V^N(\mathbf{r}) = V_\pi^N(\mathbf{r_S}) + V_\sigma(\mathbf{r_S}) + V_{\mathrm{Ss}}(\mathbf{r_S}, \mathbf{r_s}) + V_{\mathrm{ss}}(\mathbf{r_s}) \qquad (1)$$

where S and s denote the 'solute'—the emitter, and the 'solvent,' respectively. The "solvent" which involves in our case the protein and its internal and surrounding water molecules. The π-electron contribution to the emitter's Nth excited state is represented by V_π^N, while V_σ is the σ-electron contribution to the chromophore surface. V_{Ss} is the potential that couples the protein (solvent) and the chromophore and V_{ss} is the protein force field of the protein and solvent system. The surfaces V_π and V_σ are derived using the QCFF/PI method, which employs the Zero Differential Overlap (ZDO) approximation. This approximation sets $\varphi_a^*(1)\,\varphi_b(1)$ to zero for $a \neq b$ under the Pariser-Parr-Pople

approximation. This method assumes a separation between σ and π electrons in V_π^N, while V_σ is represented by an empirical force field. This approach makes the computational process more practical, facilitating the modeling of conjugated heteroatomic molecules in both ground and excited π to π* states by theoretically disentangling σ and π electrons. The QCFF/PI method is well documented and widely available.[32] It has been used extensively in studies of retinal and related systems[28,33,34] and is more efficient than QM/MM approaches. In the current study, all coelenteramide atoms are included within the QM region. The QM treatment involves a configuration interaction treatment of all the single excitations for the three highest occupied and the three lowest unoccupied orbitals. The full parameters for our systems used are those from our earlier study.[26]

The coupling potential between the solute and solvent, denoted as V_{Ss} is derived using the method presented in detail in our prior studies.[34,35] This integration involves including the electrostatic potential from the solvent (or protein) into the solute Hamiltonian, as explained in ref[34], using,

$$F_{\mu\mu} = F_{\mu\mu}^0 - \sum_k \left(q_k/\mathrm{r}_{k\mu} + \mathbf{m}_k \mathrm{r}_{k\mu}/r_{k\mu}^3\right) = F_{\mu\mu}^0 - U_\mu$$

$$F_{\mu\upsilon} = F_{\mu\upsilon}^0 \qquad (2)$$

Here $F_{\mu\upsilon}^0$ is the corresponding element of the solute's SCF matrix and *k* spans over the solvent atoms. q_k and $\mathbf{m}_k$ represent the residual charge and induced dipole on the k^{th} atom of the solvent. Overall, the second term in $F_{\mu\mu}$ captures the potential U_μ, on the μ^{th} atom from its environment. The induced dipoles are determined self-consistently and are an important part of our treatment. The solute charges are computed at each molecular dynamics (MD) step with the current **U** vector components, mirroring the present solvent setup. Concurrently, the solvent molecules respond at each step to the solute charges in the electronic state whose surface drives the given MD simulation. The approach for handling solvent and protein-induced dipoles in excited-state calculations is modeled on the procedure from eq 17 in ref[34]. Within this framework, we let the solvent's permanent and induced dipoles adapt to the charge distribution of the considered electronic state.

It's important to highlight that no existing QM/MM method offers a completely consistent way of polarizing the solvent across every excited state, as discussed in ref[34]. A perturbation approach, though suitable under certain conditions (refer to the Appendix in ref[34]), doesn't yield results matching those from eq 17 in ref[34]. In the latter, induced dipoles are polarized distinctively in each electronic state. Regardless, our approach to solvent-induced dipoles gives a more nuanced depiction of excited states within proteins and solutions.

The interaction term between the solute and solvent in Eqn. 2 encompasses the classical van der Waals interactions between solute and solvent atoms. The potential of the combined protein and solvent, V_{ss}, is characterized by the ENZYMIX force field. This includes the polarization constraints from the Surface Constrained All-Atom Solvent (SCAAS) model[31,36] and the Local Reaction Field (LRF) approach for long-range interactions.[37] The reference system was immersed in a SCAAS sphere with a 18 Å radius to solvate the system. The surface-constrained water sphere was surrounded by a 2 Å surface of Langevin dipoles and then by a bulk. The nitrogen atom in the chromophore's amide functional group was taken as center of the water sphere.

Furthermore, to ensure accurate mapping of the excited-state potential energy surface in the emission spectra calculations, we supplemented our approach with reference TD-DFT calculations for the chromophore in a water environment. We then adjusted the QCFF/PI emission spectra calculated within the protein environment by incorporating any differences observed between our QCFF/PI emission spectra and the TD-DFT results in the water environment. The adjustment is quantified as follows:

$$\lambda_{QCFF/PI}^{Total} = \lambda_{QCFF/PI}^{P} + \left(\lambda_{QCFF/PI}^{W} - \lambda_{TD-DFT}^{W}\right) \qquad (3)$$

In this equation, $\lambda_{QCFF/PI}^{Total}$ represents the total emission spectra in the protein environment. $\lambda_{QCFF/PI}^{P}$ is the emission spectra calculated within the protein environment using the QCFF/PI method. $\lambda_{QCFF/PI}^{W}$ and λ_{TD-DFT}^{W} are the emission wavelength calculated in water using the QCFF/PI and TD-DFT methods, respectively.

The ionization states of the protein residues were determined using the PDLD/S-LRA titration method (see section 2.2 for details) for the RLuc8 and its variants. Starting with

the high-resolution X-ray structure of reference 11 (PDB ID: 7OMR), we conducted an overall 200 ps relaxation run in the ground state by slowly heating the system from 5 K to 300 K. Subsequently, QCFF/PI MD simulations were performed for 10 ps in the first excited singlet state, with a 0.5 fs time step at 300 K.

The ground and excited state charges of the chromophore used in our QCFF/PI calculations were determined using the DFT method (detailed further below in section 2.3). Following this, we employed antechamber to obtain the RESP charges used in the calculations for the QM region.

2.2 The Semi-macroscopic protein dipole-Langevin dipole (PDLD/S-LRA) method

The term ionization configuration (IC) is defined as the most favored combination of protonation states of ionizable residues in a protein at certain pH. It is crucial to have a knowledge of the protonation states of the residues around the emitter as it can significantly influence the spectroscopic properties of the emitter. The IC of the studied enzyme-emitter complexes were obtained by $\mathrm{p}K_a$ calculations using the Protein Dipole Langevin Dipole (PDLD) method within the Linear Response Approximation (LRA) framework.[38] The $\mathrm{p}K_a$ of the ith ionizable residue in protein can be calculated by Eqn. (4):

$$\mathrm{p}K_{a_i}^{p} = \mathrm{p}K_{a_{int,i}}^{p} + \Delta\mathrm{p}K_{a_{int,i}}^{charges} \qquad (4)$$

Where $\mathrm{p}K_{a_{int,i}}^{p}$ refers to intrinsic $\mathrm{p}K_a$ of the ith residue, while all the other residues are kept neutral; $\Delta\mathrm{p}K_{a_{int,i}}^{charges}$ refers to change of the ith residue due to the interaction with other ionizable residues. The intrinsic $\mathrm{p}K_a$ of the ith residue can be represented as Eqn. (5):

$$\mathrm{p}K_{a_{int,i}}^{p} = \mathrm{p}K_{a_i}^{w} - \frac{\bar{q}_i}{2.3RT}\,\Delta\Delta G_{self,i}^{w\to p} \qquad (5)$$

Where $\mathrm{p}K_{a_i}^{w}$ refers to the $\mathrm{p}K_{a_i}^{w}$ of the ith residue in water; $\bar{q}_i$ refers to the charge of the residue in its ionized form (+1 for cation, -1 for anion); $\Delta\Delta G_{self,i}^{w\to p}$ represents the solvation free energy change by moving the charged form of the ith amino acid residue from water to its position in the protein when all other amino acids are neutral. This free energy

change was calculated by the PDLD method. The second term in Eqn. (4) can be obtained by Eqn. (6):

$$\Delta \mathrm{p}K_{a_{int,i}}^{charges} = -\frac{\bar{q}_i}{2.3RT}\sum_{j\neq i}\Delta G_{ij}^{p} \qquad (6)$$

Where ΔG_{ij}^{p} refers to electrostatic interactions between the i[th] amino acid in the ionized form and all other j[th] amino acid when they are assigned to be charged, as determined by the titration PDLD calculation. This correction is necessary because the intrinsic pKa deviates from the actual pKa by how the solvation of the i[th] amino acid is influenced by the presence of all other ionized residues in the protein at a given pH. The total energetics of the m[th] combination of protonation state can be expressed by Eqn. (7):

$$\Delta G^{m} = -\sum_i 1.38 q_i^m \left(\mathrm{p}K_{a_{int,i}}^{p} - \mathrm{pH}\right) + 1.66\sum_{i,j\neq i}\frac{q_i^m q_j^m}{r_{ij}\varepsilon_{ij}} \qquad (7)$$

Where ΔG^{m} denotes the free energy change of the protein transitioning from a hypothetical reference state, where all amino acids are neutral, to the m[th] ionization state. The free energy change across various ionization states were determined using the Monte Carlo method. These calculations contribute to constructing the partition function and enable the determination of ensemble-averaged charges for each ionizable residue. It's important to note that this free energy change consider only electrostatic contributions, as other effects are accounted for within the intrinsic pKa values included in the initial summation. The q_i^m and q_j^m term refer to the i[th] and j[th] charge in the m[th] charge configuration of the protein; r_{ij} refers to the distance between the centers of the i[th] and j[th] residues; ε_{ij} is the effective dielectric constant defined as Eqn. (8):

$$\varepsilon_{ij} = 1 + 60(1 - e^{-0.1 r_{ij}}) \qquad (8)$$

Eqn. (7) can be used to calculate the partition function of the protein system, and hence the average charge of i[th] residue as shown in Eqn. (9):

$$< q_i > = \frac{\sum_m q_i^m \exp\left(-\beta \Delta G^{m}\right)}{\sum_m \exp\left(-\beta \Delta G^{m}\right)} \qquad (9)$$

The average charge of all ionizable residues at certain pH is a good description of IC of a protein. To make the calculation practical and reliable, only ionizable residues within 15 Å of the binding pocket were included in the search of combinations of protonation states of the protein. In the calculation of the total energetics, intrinsic $\mathrm{p}K_a's$ of the most ionizable residues were assumed to be equal to their $\mathrm{p}K_a's$ in water. For ionizable residue clusters containing the Asp120, Asp158 and Asp162, intrinsic $\mathrm{p}K_a$ calculations were done when the emitter was in the neutral form and applied to the following average charge calculations. The reference $\mathrm{p}K_a's$ values for the aspartate residue and various states of the emitter in water, both in the ground and excited states, essential for PDLD/S-LRA calculations within the enzyme-emitter complex, were derived from DFT calculations as outlined in second 2.3.

The proton transfer (PT) mechanism involved in the bioluminescence process were obtained by $\mathrm{p}K_a$ calculations using the PDLD method. The $\mathrm{p}K_a$ calculations for specific PT donor-acceptor pairs should be considered together, which means in most of the calculations, $\mathrm{p}K_a$ of the residue was calculated while the emitter was in the neutral form. The exception was the PT process for RLuc8, in which $\mathrm{p}K_a$ (Asp162) was calculated while the emitter is in the charged phenolate form. In these calculations, the corresponding ionization configuration were used because the protonation states of nearby residues can affect the $\mathrm{p}K_a$ of interest significantly. In each calculation, $\mathrm{p}K_a$ value was obtained by averaging over 10 configurations sampled over 2 ps MD simulation with a 0.1 fs time step at 300K and a 0.3 kcal/(mol·Å^2) constraints with respect to the corresponding initial structure.

2.3 DFT Calculations

For the reference $\mathrm{p}K_a$ in water (the first term in Eqn. (5)), we utilized DFT to determine the $\mathrm{p}K_a$ of the ionizable group in the emitter and the acid species in both the ground and first excited singlet states using Eqn. (10) shown below. For the ground state, all geometries, whether in the gas or solvent phase, were optimized using the CAM-B3LYP[39]/Def2-SVP level of theory. TD-CAM-B3LYP was employed for optimizing the first

excited state and calculating the emission energies of the first three singlet excited states (nstates=3). The SMD solvation model[40] was applied for solvent phase calculations, and the GD3BJ method[41] was used for dispersion correction. Electronic and thermal energies, calculated at 298.15 K, were determined using standard statistical thermodynamic methods, incorporating unscaled frequencies and the ideal gas, rigid rotor, and harmonic oscillator approximations. The Gaussian 16 software suite[42] was used to carry out all electronic structure calculations. The charges of the chromophore in the ground and excited state used in PDLD and QCFF/PI calculations were obtained used the DFT method described above. From the resulting charges, we generated the restrained electrostatic potential (RESP)-fitted charges[43–45] using AmberTools17.[46]

Using the thermodynamic cycle (see Fig. S1 in the Supporting Information), the free energy of deprotonation (ΔG_{aq}) for the acid species in solution, given by, $HA + H_2O \leftrightharpoons H_3O^+ + A^-$ can be calculated using:

$$\Delta G_{aq} = \Delta G_g + \Delta G_{sol}(A^-) + \Delta G_{sol}(H_3O^+) - \Delta G_{sol}(HA) - \Delta G_{sol}(H_2O) \qquad (10)$$

and the corresponding $\mathrm{p}K_a$ in given by,

$$\mathrm{p}K_a = \frac{\Delta G_{aq}}{RT \ln 10} - \log[H_2O] \qquad (11)$$

The concentration of bulk water is taken as 55.4 M. It has been shown that a potential source of error in Eqn. (10) is the solvation free energy of hydronium. To address this, a value of 4.54[47] is subtracted from the $\mathrm{p}K_a$ derived from Eqn. (11).

The DFT calculated $\mathrm{p}K_a$ values for the ionizable amide, phenol, and acetic acid (which serves as a truncated model for aspartic acid) in both the ground and excited states are presented in Table S4 of the Supporting Information.

3. Results and Discussion

In our study, we utilized the high-resolution X-ray structure of RLuc8 (PDB ID: 7OMR), which was complexed with the coelenteramide chromophore, to perform a QCFF/PI MD simulation on the first excited singlet state surface. It is important to note that in the X-ray

crystal structure of RLuc8, the residue at position 162 is an alanine, resulting from a mutation of the native aspartate (referred to as RLuc8-D162A). Given that the emission spectra for the phenolate forms of the emitter have been experimentally reported in RLuc8, we reverted this alanine to its original aspartate (Asp) using a rotamer library within the Chimera software suite. Prior to analyzing the emission spectra of the studied systems, we first examined rigorously the ionization states of the protein residues.

Emission Energy of Phenolate Anion

We began by identifying the ionizable protein residues in the proximity of the chromophore in its phenolate form within 15 Å, calculating their ionization states ($\mathrm{p}K_a$) employing the PDLD/S-LRA method. At a pH of 7, our calculations revealed 11 ionized residues, that are depicted in Figure 2. Ion pairs within the protein were ionized, while distant residues remained neutral. It is crucial to mention that for the phenolate form of the emitter in RLuc8, the proximate Asp162 residue is presumed to be protonated. This is under the assumption of a proton transfer (PT) between them on the first excited state surface, given that the distance between the oxygen atom of the 6-para hydroxyphenyl group of the emitter and the protonated Asp162 residue is 2.9 Å. This close proximity suggests the likelihood of a PT process and is discussed below.

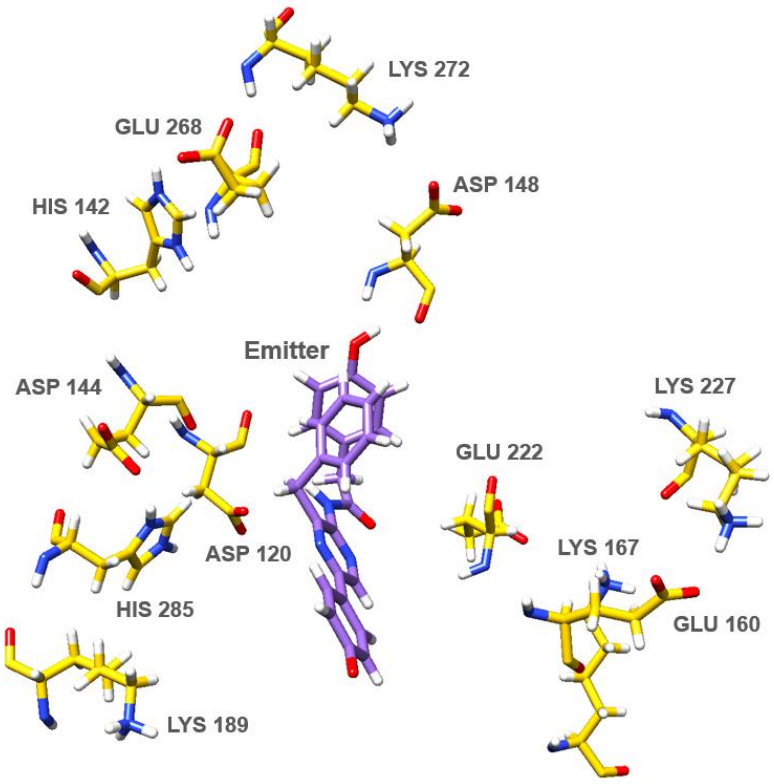

Figure 2. Assignment of ionization states to nearby ionizable residues of the chromophore in the phenolate form in RLuc8 (PDB ID: 7OMR) at pH=7.

Upon establishing the ionization states, we proceeded with QM/MM MD simulations. The quantum mechanical (QM) component was characterized using the QCFF/PI approach to define the chromophore in excited states. The MD simulations consisted of 20,000 steps with a timestep of 0.5 fs at a temperature of 300K. We recorded the emission energies of both the isolated chromophore and the chromophore influenced by MM-derived charges. The collected data points (2000 in total) were distributed across 20 bins, ranging from the lowest to the highest emission wavelengths. We then calculated the emission wavelength (λ) and their corresponding relative intensities as a fraction of occurrences per bin, normalized against the total number of data points. The emission maximum (λ_{max}) for the phenolate form in RLuc8, after correcting for the water reference value using Eqn. (3) (also refer to Table S6 for the reference emission wavelength in water), was determined to be 467 nm. This closely matches the experimentally observed

value of 480 nm. Our calculated QCFF/PI vertical emission spectrum is depicted in Figure 3. Additionally, we examined the neutral chromophore while keeping Asp162 unionized. Our calculations using the QCFF/PI approach yielded an emission maximum of 383 nm. This finding is in good accordance with the reported emission maximum of neutral coelenteramide (400 nm) observed in other bioluminescent proteins such as Ca^{2+} regulated photoprotein.[14,16,17] However, this value is significantly different from the observed emission in RLuc8. This discrepancy, along with the good agreement between the experimental and calculated emission maximum of the phenolate anion, emphasizes the importance of Asp162 protonation state. It strongly suggests that in RLuc8, the coelenteramide emitter exists in the phenolate form during its photochemical and photophysical processes.

PT Mechanism

Using gas-phase TD-DFT calculations, we carried out a preliminary investigation to study the proton transfer (PT) process using the neutral emitter and acetate as a model system. We computed the emission maximum at several fixed points along the PT reaction coordinate, which is defined by the transfer of a proton from the OH group of the phenolic fragment to the oxygen atom of the acetate (See Fig. 4). A significant red shift was observed as the neutral emitter is converted to the phenolate form, indicating that the deprotonation process has a considerable impact on the emission properties.

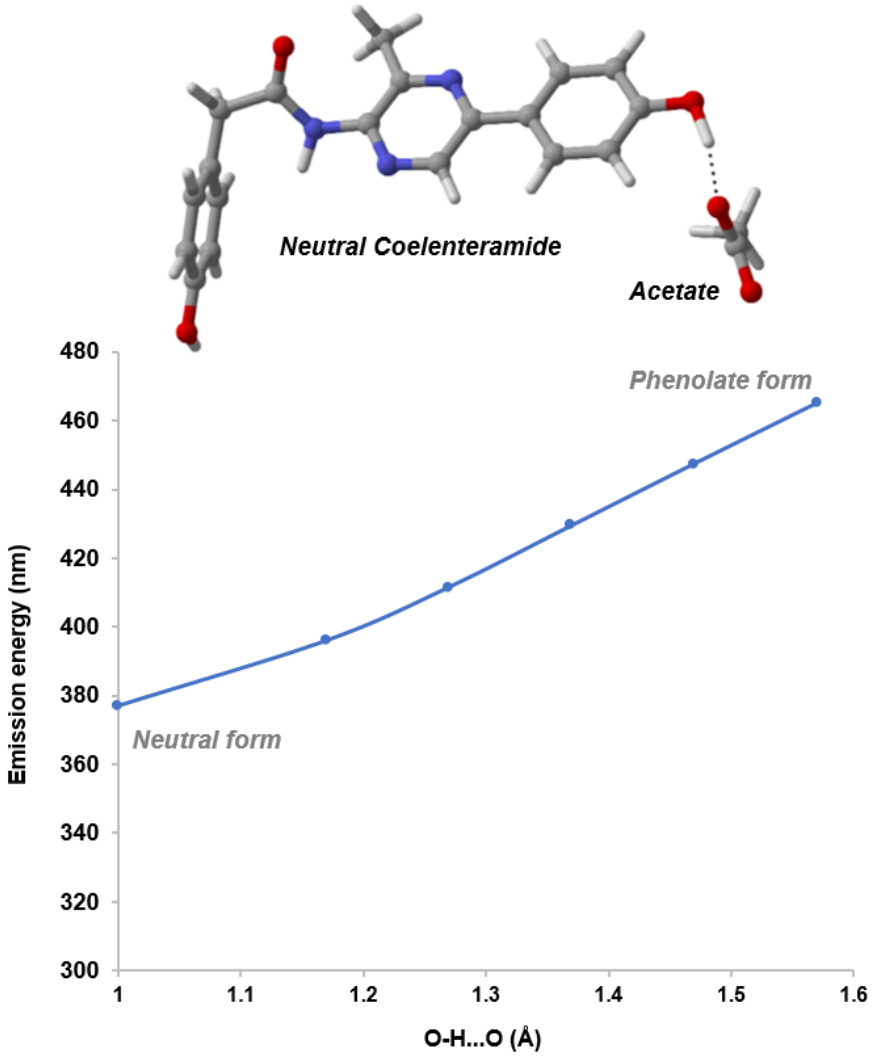

Figure 4. TD-DFT calculated emission maximum (nm) of the emitter transitioning from neutral to phenolate form at specific fixed points along the O-H bond breaking process.

Subsequently, we focused on evaluating the primary influence of the protein on the emission energy and the PT process between the neutral emitter and Asp162 by employing the PDLD/S-LRA method. This required a meticulous analysis of the PT process across both the ground and excited state free energy surfaces (ΔG), and the integration of the free energy change ($\Delta\Delta G$) between these surfaces into the QCFF/PI emission energy calculations, as illustrated in Figure 4. To delineate these free energy surfaces, we estimated the deprotonation free energy using the calculated $\mathrm{p}K_a$ values of

the neutral emitter and Asp162 in the ground state (S_0) and the first excited singlet state (S_1), applying Equation (12):

$$\Delta\Delta G_{ES-GS} = 1.38 * [(\mathrm{p}K_a(HA)^* - \mathrm{p}K_a(B^{*-})) - (\mathrm{p}K_a(HA) - \mathrm{p}K_a(B^-))] \quad (12)$$

In this equation, $(HA)^*$ and HA represent the phenolic -OH group of the neutral emitter in the excited state (ES) and ground state (GS), respectively, while B^- and (B^{*-}) denote the proton acceptor Asp162 in the GS and ES, correspondingly.

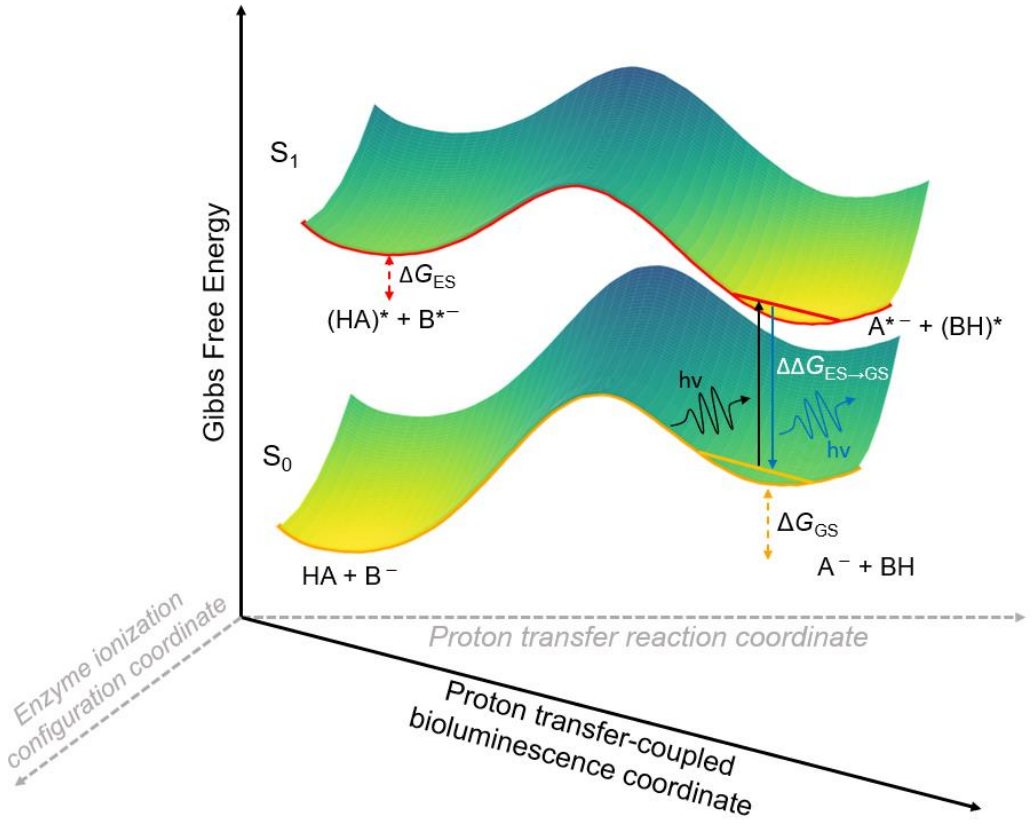

Figure 5. Proton transfer reaction profile in the ground ((S_0) and excited ((S_1) state. HA and B^- represent ionizable group of the emitter and proton acceptor (Aspartate in our case) in the ground state. The asterisk sign indicates species in the excited state (S_1). The PT process is based on $\Delta\mathrm{p}K_a$ difference calculated using PDLD/S-LRA (see Section 2.2). The $\Delta\Delta G$ term here represent the PT correction that is added to the emission energy in Eqn. 3. The Z-axis shows the ionization configuration of the protein environment, while

the diagonal axis indicates the overall incorporation of PT reaction coordinate during the bioluminescence process.

Our consensus PDLD/S-LRA pKa calculated values for the emitter and D162 at pH 7 in RLuc8 are 7.6 and 4.9, respectively, in the GS, and -0.8 and 5.1 in the ES. Utilizing Eqn. 12, this translates to reaction free energies (ΔG) of +3.7 kcal/mol in the GS and -8.1 kcalmol^{-1} in the ES, signifying that the PT reaction is energetically more favored in the ES. It should be noted that our analysis focuses solely on thermodynamic aspects, and the depicted barrier in Figure 5 serves an illustrative purpose only. Nevertheless, the PT process in the ES is typically associated with an energy barrier of a few kcal/mol, as observed in other bioluminescent proteins.[48,49] To estimate the emission spectra during the PT reaction, we incorporated the free energy change ($\Delta\Delta G$) into our calculated QCFF/PI emission maximum for the neutral emitter. This yielded an emission maximum of 455 nm, which is in reasonable agreement with the observed value of 480 nm, and closely matches with our calculated emission maximum of 467 nm predicted for the phenolate ion, thus providing evidence of the excited-state PT process in RLuc8 and that the emitter exclusively is in phenolate form.

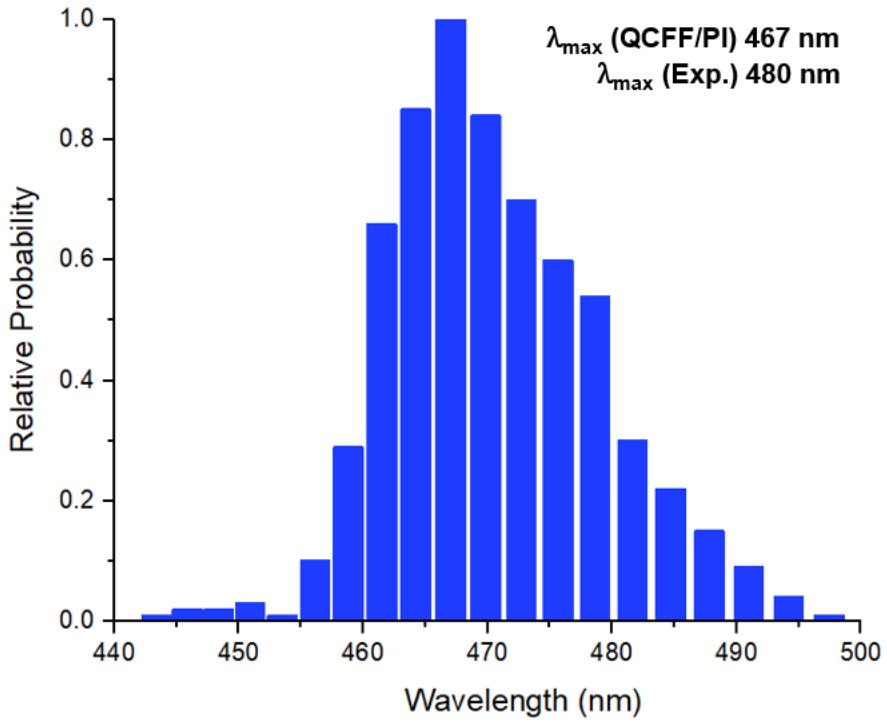

Figure 6. Calculated probability profiles for the emission spectra transition from first excited singlet state to the ground state. The profile was obtained by running trajectories on the excited state surfaces of the phenolate as emitter (when Asp162 is protonated) and evaluating the histograms of the calculated emission spectra.

Emission Energy of Amide anion

In the bioluminescence mechanism, the excited state of the amide anion is an intermediate, as outlined in the proposed reaction pathway depicted in Scheme 1. The emission peak corresponding to this intermediate species is reported for RLuc8-D120A mutant. Our PDLD titration calculation for this mutant revealed that the ionization states of the amino acids closely resemble those in the RLuc8. However, notable exceptions include the neutral state of His142 and the ionized state of Asp162 (refer to Table S2 in the Supporting Information for full ionization configurations). This suggests that preceding the transition of the amide ion to a neutral emitter via a PT process (see Scheme 1), Asp162 remains in its ionized form. The un-ionized state of His142 implies a more intricate

network of PT processes potentially involving nearby residues or the bulk solvent, as the emitter transitions from the amide ion to the neutral or phenolate form.

Moving on to our findings for the emission energy of RLuc8-D120A mutant, the calculated emission spectra (Figure 7) has a maximum at 456 nm . The position of this maximum represents a modest red shift of 26 nm, which aligns well with the experimentally observed value of 430 nm. Notably, our calculated value is consistent with the luminescence results obtained by Shimomura and Teranishi,[19] who reported an emission maximum for the amide-deprotonated emitter in the range of 435–458 nm. The correlation between the calculated emission energy and experimental data strongly suggests that the amide ion is the principal luminescent species in this mutant. This is attributed to the Asp120 position being unoccupied by aspartate, which precludes the usual proton transfer, making the formation of neutral or phenolate emitters unfavorable.

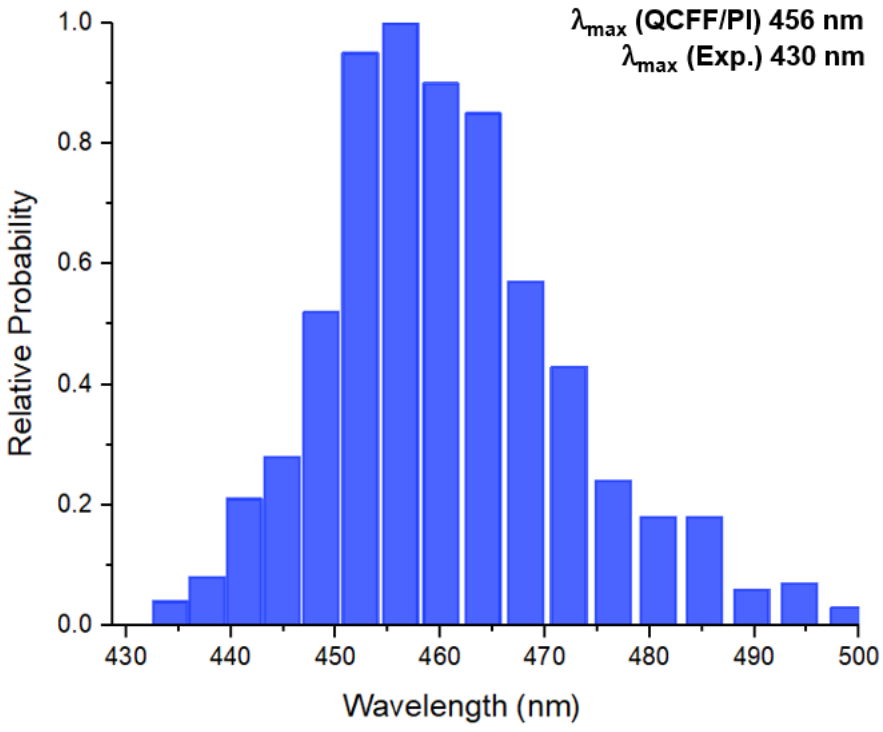

Figure 7. Calculated probability profiles for the emission from the first excited singlet state to the ground state in RLuc8-D120A. The profile was obtained by running trajectories on

the excited state surfaces of the amide ion as emitter and evaluating the histograms of the calculated emission spectra.

Emission Energy of Pyrazine anion

We next explored the pyrazine anion as a potential emitter, as identified for RLuc8-D162A. Previous research by Shimomura and colleagues[19] demonstrated that in various solvents and with alkali metals, the phenolate ion can transition to a pyrazine ion, a resonance structure of phenolate. However, this experiment was observed in the absence of protein environment. In the recent study of RLuc8-D162A,[11] the experiment was conducted in 100 mM potassium phosphate buffer, providing a high concentration of potassium ions and therefore the resonance structure of phenolate emitter might form due to the presence of this alkali metal ion. The potassium ion thus acts as a counter ion near the pyrazine ring, creating a polarized $N^{-}...K^{+}$ bond. This interaction subsequently leads to the phenolate oxygen transitioning to a keto form, a process driven by charge delocalization (refer to Scheme 2).

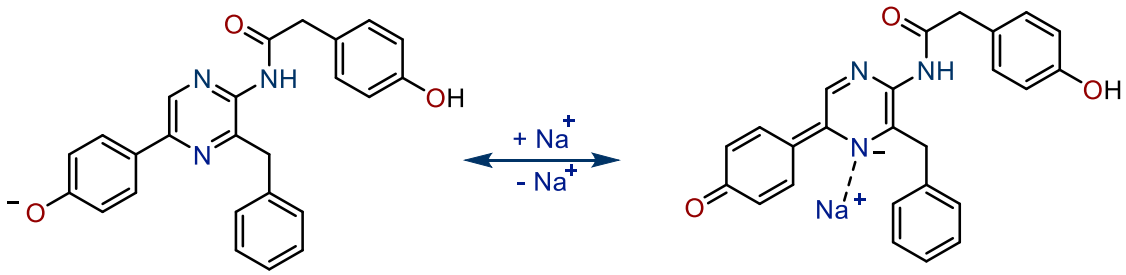

Phenolate ion ***Pyrazine ion***

Scheme 2. Resonance form between phenolate and pyrazine ion. For our system we employed Na^{+} as counter ion in the formation of pyrazine anion.

We modeled the pyrazine ion with an explicit Na^{+} positioned 2.3 Å from the pyrazine ring's nitrogen with a constraint of 3.0 kcal/mol/Å² in RLuc8-D162A. This specific distance is based on the DFT-optimized geometry of the pyrazine ion in the first singlet excited state in water. The formation of pyrazine ion necessitates the deprotonation of the OH group, initially yielding a phenolate ion, which then undergoes resonance shifting to the

pyrazine ion (as depicted in Scheme 2). Examining the X-ray crystal structure of RLuc8-D162A reveals that the nearest proton accepting residue Asp158 is located 4.9 Å from the oxygen of phenolic group of the emitter. This donor-acceptor gap is considerably lengthy for efficient proton transfer, hinting at an unfavorable process. The deprotonation of the phenolic group could potentially occur to the bulk solvent, or through a Grotthuss-type water-mediated proton transfer involving the phenolic group of the emitter and Asp158. To assess the proposed hypothesis, we investigated the emission maximum of the pyrazine ion with Asp158 in both its protonated and unprotonated states.

In the RLuc8-D162A variant, when Asp158 is unprotonated, our calculated emission maximum for the pyrazine ion is 552 nm. Conversely, when Asp158 is protonated, the emission maximum shifts to 555 nm. These predicted values, while slightly red-shifted by 32 and 35 nm respectively, align closely with the experimental value of 520 nm. This agreement suggests the presence of the pyrazine ion in this variant. Furthermore, our findings imply that D158 may serve as a proton acceptor from the chromophore, facilitated by a water-assisted Grotthuss-type mechanism as previously mentioned. It is important to note, however, that while our emission maximum is in good agreement with the observed value, the experimental study did also report a smaller peak at 400 nm, which was absent in our simulated spectra (see Fig. 8). This discrepancy may be attributed to additional structural changes in the emitter within the protein environment, possibly involving another π to π* transitions. Prior experimental studies[19] conducted in the absence of protein environment have demonstrated that the presence of a counter ion can toggle the biomolecular state of the emitter, resulting in two distinct peaks. The higher peak corresponds to the pyrazine anion, while the lower peak is linked to the amide anion. Further investigation is necessary to explore the significance of these intriguing findings within the protein environment. Additionally, considering that the experiment used a higher concentration of potassium phosphate buffer solution as mentioned above, further experimental studies focusing on the impact of buffer solution concentration effect on the emission spectra could provide insights into the biomolecular state of the emitter in RLuc8-D162A.

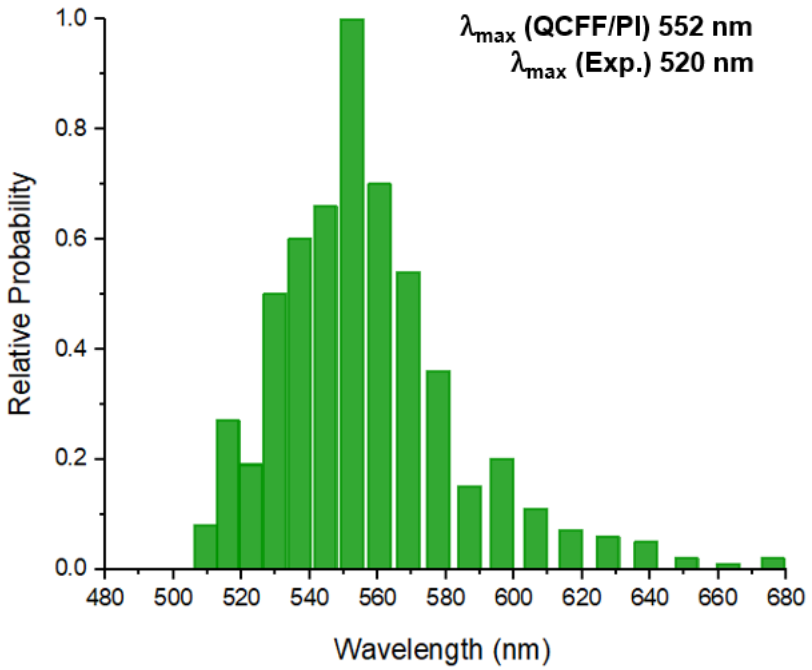

Figure 8. Calculated probability profiles for the emission spectra of pyrazine anion transition from first excited singlet state to the ground state for RLuc8-D162A.

Our study also extended to the engineered design AncFT-D160A enzyme (PDB ID: 7QXQ), known for its similarities to RLuc8-D162A in structure and active-site chemistry, yet displaying a strikingly different emission wavelength. Specifically, AncFT-D160A demonstrated a blue-shifted emission maximum at 390 nm, in stark contrast to RLuc8-D162A emission at 520 nm. The underlying cause of this shift is likely due to be the absence of an adjacent Aspartate residue, which would typically deprotonate the hydroxyl group of the R2 6-(p-hydroxyphenyl) substituent, thereby maintaining the chromophore in a neutral state. Our calculations for the neutral chromophore's emission spectra in AncFT-D160A yield a value of 375 nm, remarkably consistent with experimental observations. This finding highlights the pivotal role of hydrogen bond proton acceptor residues in determining the enzyme's emission characteristics.

4. Conclusion

In this study, we investigated the origins of bioluminescence in *Renilla* luciferase mutants. Our findings reveal that in RLuc8, the chromophore (coelenteramide) predominantly exists in its phenolate form when the nearby Asp162 is protonated. This conclusion is supported by our QCFF/PI calculations, which matches closely the experimental values of the emission maxima. Furthermore, we studied the proton transfer (PT) process that leads to the formation of the primary emitter in the RLuc8's bioluminescent reaction, utilizing both PDLD/S-LRA and QCFF/PI methods. Our calculations demonstrate that incorporating the deprotonation reaction energy between the neutral emitter and Asp162 in both the excited and ground states into the emission energy calculations accurately replicates the emission maximum of the phenolate ion. This indicates strongly that Asp162 serves as a potential proton acceptor, making the phenolate ion the dominant emitting species in RLuc8.

This study also sheds light on an important aspect of the PT process i.e., its dependency on the proton transfer process. In certain bioluminescent organisms like the firefly luciferin,[48,49] the PT of the firefly chromophore D-luciferin is known to take place in picoseconds, while the fluorescence emission takes place over nanoseconds. Considering that Asp162 in RLuc8 is merely 2.9 Å away from the hydroxyl group of the emitter, it provides the shorter pathway for PT. This proximity results in the neutral emitter being a transient species, leading to the formation of the phenolate anion. Consequently, this might explain why the emission maximum of the neutral emitter in RLuc8 was not experimentally detected.

Moreover, our calculations also provide theoretical evidence supporting the bioluminescence mechanism in the RLuc8-D120A mutant, where the light emitter is in its amide ion form. The emission maximum of this form aligns well with experimental findings. Further investigation into the bioluminescence of the RLuc8-D162A mutant reveals that the presence of a counter ion (Na^+) is essential for the formation of the pyrazine anion, with its emission maximum closely matching observed value. However, our method did not replicate the second, lower emission peak reported for RLuc8-D162A. This peak might be associated with another biomolecular state of the emitter that our approach did not capture, suggesting a need for further investigation. More sophisticated

theoretical approaches will be required to fully understand and assess the significance of these intriguing results. Additionally, our analysis of the AncFT-D160A engineered enzyme, which is structurally analogous to RLu8-D162A yet exhibiting a distinctly blue-shifted emission maximum, shows it lacks aspartate residues on the rim of catalytic pocket that can accept protons. This inhibits the deprotonation of the hydroxyl group on the R2 6-(p-hydroxyphenyl) substituent of the emitter, thereby maintaining the emitter in a neutral state. Our predicted emission spectra for this neutral form align well with experimental results, and this might explain the differences in observed emission spectra. In summary, our methods offer an efficient means to study the bioluminescence properties, as well as the proton transfer (PT) mechanism, in a manner that is considerably less resource-intensive than conventional quantum mechanics/molecular mechanics (QM/MM) methods and proves to be a valuable tool for studying PT processes in the luminescent reactions of photoproteins.

Notes

The authors declare no competing financial interest.

Acknowledgements

This work is supported by the National Institute of Health R35 GM122472, the National Science Foundation Grant MCB 2142727.

References

(1) Lorenz, W. W.; McCann, R. O.; Longiaru, M.; Cormier, M. J. Isolation and Expression of a cDNA Encoding Renilla Reniformis Luciferase. *Proc. Natl. Acad. Sci.* **1991**, *88* (10), 4438–4442. https://doi.org/10.1073/pnas.88.10.4438.

(2) J. Syed, A.; C. Anderson, J. Applications of Bioluminescence in Biotechnology and Beyond. *Chem. Soc. Rev.* **2021**, *50* (9), 5668–5705. https://doi.org/10.1039/D0CS01492C.

(3) Xu, T.; Close, D.; Handagama, W.; Marr, E.; Sayler, G.; Ripp, S. The Expanding Toolbox of In Vivo Bioluminescent Imaging. *Front. Oncol.* **2016**, *6*.

(4) Carrasco-López, C.; Lui, N. M.; Schramm, S.; Naumov, P. The Elusive Relationship between Structure and Colour Emission in Beetle Luciferases. *Nat. Rev. Chem.* **2021**, *5* (1), 4–20. https://doi.org/10.1038/s41570-020-00238-1.

(5) Khakhar, A.; Starker, C. G.; Chamness, J. C.; Lee, N.; Stokke, S.; Wang, C.; Swanson, R.; Rizvi, F.; Imaizumi, T.; Voytas, D. F. Building Customizable Auto-Luminescent Luciferase-Based Reporters in Plants. *eLife* **2020**, *9*, e52786. https://doi.org/10.7554/eLife.52786.

(6) Xie, W. J.; Liu, D.; Wang, X.; Zhang, A.; Wei, Q.; Nandi, A.; Dong, S.; Warshel, A. Enhancing Luciferase Activity and Stability through Generative Modeling of Natural Enzyme Sequences. *Proc. Natl. Acad. Sci.* **2023**, *120* (48), e2312848120. https://doi.org/10.1073/pnas.2312848120.

(7) Navizet, I. QM/MM Study of Bioluminescent Systems. In *QM/MM Studies of Light-responsive Biological Systems*; Andruniów, T., Olivucci, M., Eds.; Challenges and Advances in Computational Chemistry and Physics; Springer International Publishing: Cham, 2021; pp 227–270. https://doi.org/10.1007/978-3-030-57721-6_5.

(8) Hori, K.; Wampler, J. E.; Matthews, J. C.; Cormier, M. J. Bioluminescence of Renilla Reniformis. XIII. Identification of the Product Excited States during the Chemiluminescent and Bioluminescent Oxidation of Renilla (Sea Pansy) Luciferin and Certain of Its Analogs. *Biochemistry* **1973**, *12* (22), 4463–4468. https://doi.org/10.1021/bi00746a025.

(9) Matthews, J. C.; Hori, K.; Cormier, M. J. Purification and Properties of Renilla Reniformis Luciferase. *Biochemistry* **1977**, *16* (1), 85–91. https://doi.org/10.1021/bi00620a014.

(10) Matthews, J. C.; Hori, K.; Cormier, M. J. Substrate and Substrate Analogue Binding Properties of Renilla Luciferase. *Biochemistry* **1977**, *16* (24), 5217–5220. https://doi.org/10.1021/bi00643a009.

(11) Schenkmayerova, A.; Toul, M.; Pluskal, D.; Baatallah, R.; Gagnot, G.; Pinto, G. P.; Santana, V. T.; Stuchla, M.; Neugebauer, P.; Chaiyen, P.; Damborsky, J.; Bednar, D.; Janin, Y. L.; Prokop, Z.; Marek, M. Catalytic Mechanism for Renilla-Type Luciferases. *Nat. Catal.* **2023**, *6* (1), 23–38. https://doi.org/10.1038/s41929-022-00895-z.

(12) Head, J. F.; Inouye, S.; Teranishi, K.; Shimomura, O. The Crystal Structure of the Photoprotein Aequorin at 2.3 A Resolution. *Nature* **2000**, *405* (6784), 372–376. https://doi.org/10.1038/35012659.

(13) Liu, Z. J.; Vysotski, E. S.; Chen, C. J.; Rose, J. P.; Lee, J.; Wang, B. C. Structure of the Ca2+-Regulated Photoprotein Obelin at 1.7 A Resolution Determined Directly from Its Sulfur Substructure. *Protein Sci. Publ. Protein Soc.* **2000**, *9* (11), 2085–2093. https://doi.org/10.1110/ps.9.11.2085.

(14) Vysotski, E. S.; Lee, J. Ca2+-Regulated Photoproteins: Structural Insight into the Bioluminescence Mechanism. *Acc. Chem. Res.* **2004**, *37* (6), 405–415. https://doi.org/10.1021/ar0400037.

(15) Vysotski, E. S.; Liu, Z.-J.; Markova, S. V.; Blinks, J. R.; Deng, L.; Frank, L. A.; Herko, M.; Malikova, N. P.; Rose, J. P.; Wang, B.-C.; Lee, J. Violet Bioluminescence and Fast Kinetics from W92F Obelin: Structure-Based Proposals for the Bioluminescence Triggering and the Identification of the Emitting Species. *Biochemistry* **2003**, *42* (20), 6013–6024. https://doi.org/10.1021/bi027258h.

(16) Deng, L.; Markova, S. V.; Vysotski, E. S.; Liu, Z.-J.; Lee, J.; Rose, J.; Wang, B.-C. Crystal Structure of a Ca2+-Discharged Photoprotein: Implications for Mechanisms of the Calcium Trigger and Bioluminescence. *J. Biol. Chem.* **2004**, *279* (32), 33647–33652. https://doi.org/10.1074/jbc.M402427200.

(17) Chen, S.; Navizet, I.; Lindh, R.; Liu, Y.; Ferré, N. Hybrid QM/MM Simulations of the Obelin Bioluminescence and Fluorescence Reveal an Unexpected Light Emitter. *J. Phys. Chem. B* **2014**, *118* (11), 2896–2903. https://doi.org/10.1021/jp412198w.

(18) McCapra, F.; Hart, R. The Origins of Marine Bioluminescence. *Nature* **1980**, *286* (5774), 660–661. https://doi.org/10.1038/286660a0.

(19) Shimomura, O.; Teranishi, K. Light-Emitters Involved in the Luminescence of Coelenterazine. *Lumin. J. Biol. Chem. Lumin.* **2000**, *15* (1), 51–58. https://doi.org/10.1002/(SICI)1522-7243(200001/02)15:1<51::AID-BIO555>3.0.CO;2-J.

(20) Shimomura, O.; Masugi, T.; Johnson, F. H.; Haneda, Y. Properties and Reaction Mechanism of the Bioluminescence System of the Deep-Sea Shrimp Oplophorus Gracilorostris. *Biochemistry* **1978**, *17* (6), 994–998. https://doi.org/10.1021/bi00599a008.

(21) Ohmiya, Y.; Hirano, T. Shining the Light: The Mechanism of the Bioluminescence Reaction of Calcium-Binding Photoproteins. *Chem. Biol.* **1996**, *3* (5), 337–347. https://doi.org/10.1016/s1074-5521(96)90116-7.

(22) Loening, A. M.; Fenn, T. D.; Wu, A. M.; Gambhir, S. S. Consensus Guided Mutagenesis of Renilla Luciferase Yields Enhanced Stability and Light Output. *Protein Eng. Des. Sel. PEDS* **2006**, *19* (9), 391–400. https://doi.org/10.1093/protein/gzl023.

(23) Loening, A. M.; Fenn, T. D.; Gambhir, S. S. Crystal Structures of the Luciferase and Green Fluorescent Protein from Renilla Reniformis. *J. Mol. Biol.* **2007**, *374* (4), 1017–1028. https://doi.org/10.1016/j.jmb.2007.09.078.

(24) Schenkmayerova, A.; Pinto, G. P.; Toul, M.; Marek, M.; Hernychova, L.; Planas-Iglesias, J.; Daniel Liskova, V.; Pluskal, D.; Vasina, M.; Emond, S.; Dörr, M.; Chaloupkova, R.; Bednar, D.; Prokop, Z.; Hollfelder, F.; Bornscheuer, U. T.; Damborsky, J. Engineering the Protein Dynamics of an Ancestral Luciferase. *Nat. Commun.* **2021**, *12* (1), 3616. https://doi.org/10.1038/s41467-021-23450-z.

(25) Warshel, A. The QCFF/PI+MCA Program Package Efficiency and Versatility in Molecular Mechanics. *Comput. Chem.* **1977**, *1* (3), 195–202. https://doi.org/10.1016/0097-8485(77)85010-9.

(26) Warshel, A.; Lappicirella, A. Calculations of Ground- and Excited-State Potential Surfaces for Conjugated Heteroatomic Molecules. *J. Am. Chem. Soc.* **1981**, *103* (16), 4664–4673. https://doi.org/10.1021/ja00406a002.

(27) Warshel, A. Quantum Mechanical Consistent Force Field (QCFF/PI) Method: Calculations of Energies, Conformations and Vibronic Interactions of Ground and Excited States of Conjugated Molecules. *Isr. J. Chem.* **1973**, *11* (5), 709–717. https://doi.org/10.1002/ijch.197300067.

(28) Warshel, A.; Karplus, M. Calculation of .Pi..Pi.* Excited State Conformations and Vibronic Structure of Retinal and Related Molecules. *J. Am. Chem. Soc.* **1974**, *96* (18), 5677–5689. https://doi.org/10.1021/ja00825a001.

(29) Warshel, A.; Karplus, M. Calculation of Ground and Excited State Potential Surfaces of Conjugated Molecules. I. Formulation and Parametrization. *J. Am. Chem. Soc.* **1972**, *94* (16), 5612–5625. https://doi.org/10.1021/ja00771a014.

(30) Warshel, A.; Chu, Z. T.; Villa, J.; Strajbl, M.; Schutz, C.; Shurki, A.; Vicatos, S.; Plotnikov, N.; Schopf, P. *Molaris-Xg, Version 9.15*; University of Southern California: Los Angeles, 2012.

(31) Lee, F. S.; Chu, Z. T.; Warshel, A. Microscopic and Semimicroscopic Calculations of Electrostatic Energies in Proteins by the POLARIS and ENZYMIX Programs. *J. Comput. Chem.* **1993**, *14* (2), 161–185. https://doi.org/10.1002/jcc.540140205.

(32) Warshel, A.; Levitt, M. *Program for the ConsistentForce Field EValuation of Equilibrium Geometries and VibrationalFrequencies of Molecules.*; Quantum Chemistry ProgramExchange; Indiana University: Bloomington, IN, 1974; Vol. QCPE 247.

(33) Warshel, A.; Chu, Z. T. Nature of the Surface Crossing Process in Bacteriorhodopsin: Computer Simulations of the Quantum Dynamics of the Primary Photochemical Event. *J. Phys. Chem. B* **2001**, *105* (40), 9857–9871. https://doi.org/10.1021/jp010704a.

(34) Luzhkov, V.; Warshel, A. Microscopic Calculations of Solvent Effects on Absorption Spectra of Conjugated Molecules. *J. Am. Chem. Soc.* **1991**, *113* (12), 4491–4499. https://doi.org/10.1021/ja00012a018.

(35) Warshel, A. Bicycle-Pedal Model for the First Step in the Vision Process. *Nature* **1976**, *260* (5553), 679–683. https://doi.org/10.1038/260679a0.

(36) King, G.; Warshel, A. A Surface Constrained All-atom Solvent Model for Effective Simulations of Polar Solutions. *J. Chem. Phys.* **1989**, *91* (6), 3647–3661. https://doi.org/10.1063/1.456845.

(37) Lee, F. S.; Warshel, A. A Local Reaction Field Method for Fast Evaluation of Long-range Electrostatic Interactions in Molecular Simulations. *J. Chem. Phys.* **1992**, *97* (5), 3100–3107. https://doi.org/10.1063/1.462997.

(38) Sham, Y. Y.; Chu, Z. T.; Warshel, A. Consistent Calculations of pKa's of Ionizable Residues in Proteins: Semi-Microscopic and Microscopic Approaches. *J. Phys. Chem. B* **1997**, *101* (22), 4458–4472. https://doi.org/10.1021/jp963412w.

(39) Yanai, T.; Tew, D. P.; Handy, N. C. A New Hybrid Exchange–Correlation Functional Using the Coulomb-Attenuating Method (CAM-B3LYP). *Chem. Phys. Lett.* **2004**, *393* (1), 51–57. https://doi.org/10.1016/j.cplett.2004.06.011.

(40) Marenich, A. V.; Cramer, C. J.; Truhlar, D. G. Performance of SM6, SM8, and SMD on the SAMPL1 Test Set for the Prediction of Small-Molecule Solvation Free Energies. *J. Phys. Chem. B* **2009**, *113* (14), 4538–4543. https://doi.org/10.1021/jp809094y.

(41) Grimme, S. Supramolecular Binding Thermodynamics by Dispersion-Corrected Density Functional Theory. *Chem. – Eur. J.* **2012**, *18* (32), 9955–9964. https://doi.org/10.1002/chem.201200497.

(42) M. J. Frisch. *Gaussian 16 Revis. A03 Gaussian Inc Wallingford CT* **2016**.

(43) Bayly, C. I.; Cieplak, P.; Cornell, W.; Kollman, P. A. A Well-Behaved Electrostatic Potential Based Method Using Charge Restraints for Deriving Atomic Charges: The RESP Model. *J. Phys. Chem.* **1993**, *97* (40), 10269–10280. https://doi.org/10.1021/j100142a004.

(44) Cieplak, P.; Cornell, W. D.; Bayly, C.; Kollman, P. A. Application of the multimolecule and multiconformational RESP methodology to biopolymers: Charge derivation for DNA, RNA, and proteins. *J. Comput. Chem.* **1995**, *16* (11), 1357–1377. https://doi.org/10.1002/jcc.540161106.

(45) Cornell, W. D.; Cieplak, P.; Bayly, C. I.; Kollman, P. A. Application of RESP Charges to Calculate Conformational Energies, Hydrogen Bond Energies, and Free Energies of Solvation. *J. Am. Chem. Soc.* **1993**, *115* (21), 9620–9631. https://doi.org/10.1021/ja00074a030.

(46) *The Amber biomolecular simulation programs - Case - 2005 - Journal of Computational Chemistry - Wiley Online Library*. https://onlinelibrary.wiley.com/doi/full/10.1002/jcc.20290 (accessed 2023-09-22).

(47) Pliego, J. R. Thermodynamic Cycles and the Calculation of pKa. *Chem. Phys. Lett.* **2003**, *367* (1), 145–149. https://doi.org/10.1016/S0009-2614(02)01686-X.

(48) Presiado, I.; Erez, Y.; Huppert, D. Excited-State Intermolecular Proton Transfer of Firefly Luciferin III. Proton Transfer to a Mild Base. *J. Phys. Chem. A* **2010**, *114* (51), 13337–13346. https://doi.org/10.1021/jp107360d.

(49) Erez, Y.; Presiado, I.; Gepshtein, R.; Huppert, D. Excited-State Intermolecular Proton Transfer of Firefly Luciferin IV. Temperature and pH Dependence. *J. Phys. Chem. A* **2011**, *115* (9), 1617–1626. https://doi.org/10.1021/jp110889v.